

Article

Artificial Neural Network Modeling to Predict the Effect of Milling Time and TiC Content on the Crystallite Size and Lattice Strain of Al7075-TiC Composites Fabricated by Powder Metallurgy

Mohammad Azad Alam ^{1,*}, Hamdan H. Ya ^{1,*}, Mohammad Azeem ¹, Mohammad Yusuf ², Imtiaz Ali Soomro ¹, Faisal Masood ³, Imtiaz Ahmed Shozib ⁴, Salit M. Sapuan ^{5,6} and Javed Akhter ⁷

- ¹ Mechanical Engineering Department, Universiti Teknologi PETRONAS, Seri Iskandar 32610, Malaysia; mohammad_18000380@utp.edu.my (M.A.); imtiaz_17007503@utp.edu.my (I.A.S.)
- ² Chemical Engineering Department, Universiti Teknologi PETRONAS, Seri Iskandar 32610, Malaysia; mohd_18002092@utp.edu.my
- ³ Electrical Engineering Department, Universiti Teknologi PETRONAS, Seri Iskandar 32610, Malaysia; faisal_17001061@utp.edu.my
- ⁴ Mechanical Engineering Department, Rochester Institute of Technology, Rochester, NY 14623, USA; ahmed_19001670@utp.edu.my
- ⁵ Laboratory of Biocomposite Technology, Institute of Tropical Forestry and Forest Products, Universiti Putra Malaysia, Serdang 43400, Malaysia; sapuan@upm.edu.my
- ⁶ Department of Mechanical and Manufacturing Engineering, Universiti Putra Malaysia, Serdang 43400, Malaysia
- ⁷ Department of Mechatronics Engineering, Chakwal Campus, University of Engineering and Technology Taxila, Chakwal 47050, Pakistan; javed.akhter@uettaxila.edu.pk
- * Correspondence: mohammad_18000664@utp.edu.my (M.A.A.); hamdan.ya@utp.edu.my (H.H.Y.)



Citation: Alam, M.A.; Ya, H.H.; Azeem, M.; Yusuf, M.; Soomro, I.A.; Masood, F.; Shozib, I.A.; Sapuan, S.M.; Akhter, J. Artificial Neural Network Modeling to Predict the Effect of Milling Time and TiC Content on the Crystallite Size and Lattice Strain of Al7075-TiC Composites Fabricated by Powder Metallurgy. *Crystals* **2022**, *12*, 372. <https://doi.org/10.3390/cryst12030372>

Academic Editor: Chongchong Qi

Received: 19 February 2022

Accepted: 7 March 2022

Published: 10 March 2022

Publisher's Note: MDPI stays neutral with regard to jurisdictional claims in published maps and institutional affiliations.



Copyright: © 2022 by the authors. Licensee MDPI, Basel, Switzerland. This article is an open access article distributed under the terms and conditions of the Creative Commons Attribution (CC BY) license (<https://creativecommons.org/licenses/by/4.0/>).

Abstract: In the study, Al7075-TiC composites were synthesized by using a novel dual step blending process followed by cold pressing and sintering. The effect of ball milling time on the microstructure of the synthesized composite powder was characterized using X-ray diffraction measurements (XRD), scanning electron microscopy (SEM), energy dispersive spectroscopy (EDS), and transmission electron microscopy (TEM). Subsequently, the integrated effects of the two-stage mechanical alloying process were investigated on the crystallite size and lattice strain. The crystallite size and lattice strain of blended samples were calculated using the Scherrer method. The prediction of the crystallite size and lattice strain of synthesized composite powders was conducted by an artificial neural network technique. The results of the mixed powder revealed that the particle size and crystallite size improved with increasing milling time. The particle size of the 3 h-milled composites was 463 nm, and it reduces to 225 nm after 7 h of milling time. The microhardness of the produced composites was significantly improved with milling time. Furthermore, an artificial neuron network (ANN) model was developed to predict the crystallite size and lattice strain of the synthesized composites. The ANN model provides an accurate model for the prediction of lattice parameters of the composites.

Keywords: mechanical alloying; Al7075/TiC composites; microhardness; artificial neural networks; crystallite size; lattice strain

1. Introduction

The quest for fuel-saving and cost-effective materials with attractive structural and mechanical properties has led to the development of aluminum matrix composites for automotive and aircraft applications. In various engineering fields, such as transportation, aviation, and the military, there is a growing need for new and advanced materials with superior physical and mechanical properties. This is because single monolithic materials do not display combined structural properties such as hardness and ductility. To address this

issue, metal matrix composites (MMCs) display great potential in combining or altering the desired properties of a highly reinforced ductile and resilient matrix [1–4]. Hence, the development of high-performance metal-based composite materials is important for modern technological applications due to the growing demand for lighter materials with enhanced mechanical properties [4,5]. Composites of the particle-reinforced aluminum alloy-based metal matrix (AMMCs) are highly desirable materials for aircraft and automotive applications. For instance, Al7075 is an aluminum alloy of high performance with reasonably good mechanical strength [6–10]. The demand for aluminum composites has grown in recent years owing to their unique features that display substantial weight reduction due to high strength-to-weight ratio, excellent dimensional stability, strong physical isotropic characteristics, and enhanced mechanical and physical properties such as elastic rigidity, hardness, strength, characteristics of cyclic fatigue, tribological properties, and creep resistance [11–15]. Aluminum alloy based MMCs reinforced with titanium carbide (TiC) particles have been particularly suitable for aircraft, automotive, defense, and other structural applications due to their excellent mechanical and physical characteristics. TiC has been widely used due to its superior hardness, low density, good elastic modulus, wettability with aluminum, and high-temperature stability [12,16–19]. The studies related to Al7075 as a matrix and TiC particles as reinforcements are illustrated in Table 1.

Table 1. Aluminum-based composites produced by mechanical alloying.

S.No.	Materials		Preparation Technique	Major Outcomes	References
	Matrix	Reinforcements with CONTENTS			
1	Al7075	TiC (5%)	Mechanical alloying (MA) followed by hot pressing (10 h, 30 h, and 50 h).	Significant improvement in crystallite size, accumulations in lattice strains, and high mechanical properties.	[6]
2	Al7075	ZrO ₂ (2%, and 5%)	Mechanical alloying by three different mills (planetary, horizontal attritor, and shaker), 15 h.	Considerable improvement in crystallite size and enhancement in lattice strain.	[20]
3	Al7075	GNP (0, 1, and 2%)	Mechanical alloying in high energy SPEX mill (for 2.5, 5, and 10 h) followed by consolidation.	Improvement in particle size and mechanical properties (hardness and strength).	[21]
4	AA6061	TiC (1, 1.5, 2 wt.%)	Mechanical alloying with a milling time of 30 h.	The structural and mechanical properties improved.	[16]
5	AA6005 A	TiC (1.5, 3, and 6 vol. %)	High energy ball milling for different milling times, in the range from 1 to 10 h.	The effect of the milling process is greater than that of the reinforcement.	[22]
6	Al7075	TiC (5 %)	Turbula mixing	Reduction in crystallite size	[23]
7	Al7075	TiC (4 wt.%)	(Turbula mixing + high energy planetary ball mill) for 3, 5, and 7 h MA.	Significant improvement in crystallite size and accumulation in lattice strain achieved. Microhardness improved.	Present study

The synthesis of AMMCs are not only affected by reinforcement-related variables, but also by the production routes and their associated conditions [24]. To provide a precisely customized performance for demanding applications, primary emphasis is given to the systematic synthesis and control of material crystal structure and microstructure. AMMCs

reinforced with micron and nanoparticles can be synthesized following different routes that can be divided into two classes, namely solid-state and liquid-state processing. Typically, solid-state methods include powder metallurgy (PM) processes [1]. PM techniques include powder processing, where a base metal powder is mixed with reinforcement particles or fibers by mechanical alloying, the compaction stage, and the final forming stage (sintering, extrusion) to obtain a bulk composite [25,26]. The ball milling method enables a homogeneous mixture to be obtained with a good distribution of reinforced particles in the metal matrix. This step is particularly significant for microns and nanoparticles due to their potential to agglomerate [27–30]. During the high energy ball milling (HEBM) process of different powders, fracture and extreme deformation of the powder particles occur, thus causing significant microstructural changes such as the reduction in crystallite size, which results in major grain refinement and accretion of the lattice strain (lattice distortions) of the Al7075 matrix [31]. This refinement occurs due to the existence of lattice defects, especially dislocation density within the grains, destruction, and replication of dislocations in the unit cell to build tiny angle boundaries at a fixed strain level and formation of sub-grains in the micron and nanometric size range [11]. Milling parameters such as milling time, milling speed, milling container and atmosphere, type of milling, the ball-to-powder content ratio (BPR) for ball milling, and operation mode are vital to obtain a minimum feasible grain size and distribution of reinforcement particles in the matrix [32]. Hence, the correct assessment of process parameters is essential to ensure that the features of the Turbula-mixed and ball-milled powder support the consolidation process and strengthen the final characteristics of the composite materials. During the Turbula mixing, the powders particles are exposed to drop and impact effect by the Turbula mixer with a mechanism combining translation, inversion, and rotation motions. This drop impact force moves to the powders with quick instantaneous strikes, which, in turn, deforms the powders and are reduced to their size [33]. Thus, combining both schemes, i.e., the Turbula mixing and mechanical alloying, to produce the composites powder and to see their effects on particles could be interesting. Some researchers have already studied the combined mixing technique, i.e., Turbula mixing and mechanical alloying, for producing composites or alloys [34–36].

In recent years, artificial neural networks (ANN) have evolved as a new branch of artificial intelligence in computing, and they have been utilized in a variety of engineering applications [37–39]. An artificial neural network (ANN) is a modeling technique that is based on the artificial intelligence-supervised learning algorithm. ANN is based on the neural structure of the human brain, which processes data among several neurons [40,41]. The neuron is the basic unit in ANN. These neurons are associated with one another based on a weight factor that decides the strength of the interconnections and the influence of that interconnection on the accompanying neurons. The neural networks can be trained to perform a specific function by changing the values of the weight factors among the neurons, either from the data obtained outside the network or in response to the feedback by the neuron itself. This characteristic feature enables ANN to acquire memory by learning. The ANN algorithm links neurons in different layers to carry out its functions. Various studies have been performed on the prediction of the physical and mechanical characteristics of several composites [41–47].

The research question for the present work is as follows: What are the constitutional and microstructural changes because of mechanical alloying of Al7075/TiC composites? How does the milling time affect the crystallite size and lattice strain microhardness of aluminum-based composites? What are the advantages of using a combined blending process? Literature studies have indicated that Al alloy-based composites have been developed by the mechanical alloying (MA) method. Even though the effect of milling parameters on the mechanical and physical properties of aluminum composites has been investigated in several studies [48–50]. Also, the comparative study on different kinds of ball mills for the synthesis of aluminum alloy-based composites has also been studied [20]. In a recent study, the optimization of tribological behavior of powder metallurgy processed Al7075/SiC composites were conducted by using ANN and ANOVA [51]. However, the

combination of two simultaneously blending processes (Turbula mixed + MA) has not been analyzed for the development of the Al7075/TiC composite powder. Moreover, the influence of milling time on the powder morphology and crystal structure of milled Al7075/TiC composite powders is less investigated. The ANN prediction technique was rarely employed for the prediction of the response of newly mixed composites for different milling times. Therefore, the main objective of the present work is the development of the Al7075/4 wt.% TiC composite powder using a two-stage blending process, their detailed characterizations (particle morphology, the variation of crystallite size and lattice strain, and the effect of milling time on the crystallite size and lattice strain of the milled composites powder), and to investigate the effect of milling time on the microhardness behavior of produced Al7075/4 wt.% TiC composites. Another objective is to develop an artificial neural network model to correctly predict the crystallite size and lattice strain of the two-stage mixed composites.

2. Materials and Methods

The methodology steps for the present study are as follows:

- Synthesis of composite powders by dual blending scheme.
- Determination of crystallite size, lattice strain, and their predictions using ANN.
- Microstructural characterizations and analysis of blended composite powders.
- Fabrication of bulk composites and investigations on microhardness behavior.

2.1. Starting Materials

The matrix material Al7075 and reinforcement TiC were utilized for the fabrication of composite powder. The elemental chemical compositions of matrix Al7075 are expressed in Table 2. The spherical-shaped Al7075 powder with an average particle size of 15 μm was purchased from the CNPC Powder Co., Ltd., Shanghai, China.

Table 2. Al7075 alloy compositions.

Elements	Si	Cr	Mn	Fe	Cu	Mg	Ai	Zn	Al
wt.%	0.087	0.185	0.08	0.092	1.56	2.31	0.05	5.72	Bal.

The reinforcement chosen for composite fabrication was titanium carbide (98.8% purity, with a nominal average particle size of <800 nm, supplied by Nova Scientific Malaysia).

2.2. Blending of Matrix and Reinforcement Powders

The Al alloy-based metal matrix composite (Al7075/4 wt.% TiC) particles were synthesized using the two-stage blending process. In the first stage, the blending of the matrix and reinforcement powders was performed for 1 h using the Turbula mixer (Willy A. Bachofen AG, Maschinenfabrik, 16000-000-6223, Switzerland). In the second stage, a planetary mono ball mill (FRITSCH, Pulverisette, A-1552, Germany) was utilized for the high-energy ball milling of premixed powders obtained from the first stage. A schematic illustration is shown for the two-stage mixing process in Figure 1. The stainless-steel balls (10 mm in diameter and 15.5 g weight) were utilized for mechanical alloying with a ball-to-powder ratio (BPR) of 10:1, and the rotation speed of the ball mill was maintained at 300 rpm. The milling of the powders was performed for three different milling time intervals at 3, 5, and 7 h. Stearic acid (2 wt.%) was used as the process controlling agent (PCA) during the milling process to prevent any unnecessary cold welding of the particles among themselves or on the inner surface of the mixer wall and to inhibit agglomeration [8,17,52].

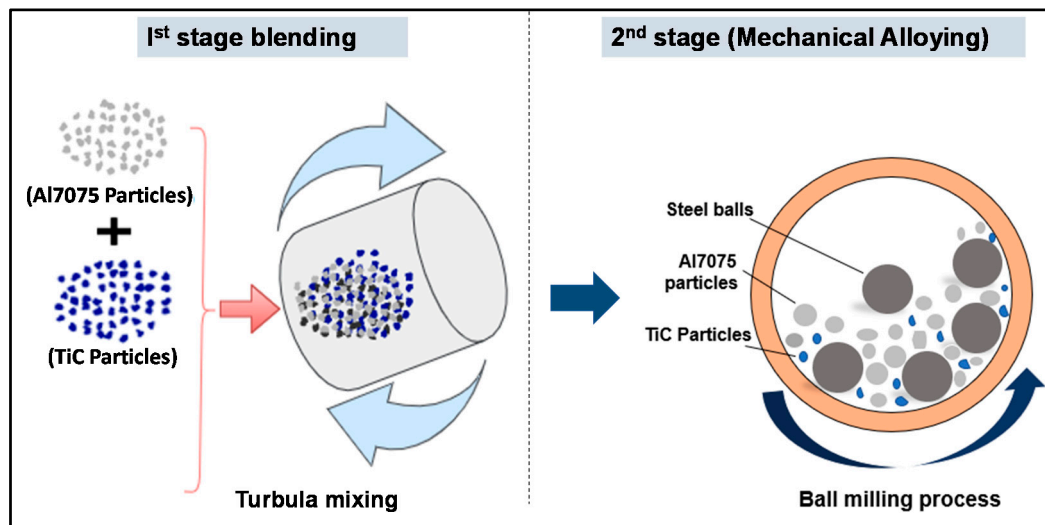


Figure 1. Schematic illustration of the novel two-stage blending process for homogeneous mixing of the matrix and reinforcement powders.

To prevent major temperature increases, 10 min of milling was alternated with 10 min of cooling [16]. The milled powder samples obtained at different time intervals were dried at 70 °C for 12 h in a vacuum drying oven for microstructural characterization.

2.3. Microhardness Measurement and Microstructural Characterization

The microhardness measurement for all the sintered composites was completed by using a Vickers hardness tester (Leco LM 247 AT, Saint Joseph, MO, USA). The standard test method (ASTM E92-82) was followed for the measurement of microhardness. The test was conducted at ambient temperature, and the indentation load was kept at 500 gf with a dwell time of 15 s. At least five microhardness readings were recorded at different locations of each test specimen, and average values were taken into consideration. The characterization of reinforcement TiC powder and the composite samples for different milling times were also performed using a transmission electron microscope (Philips/FEI Tecnai F30, Hillsboro, OR, USA) operated at 300 kV

2.4. Crystal Structure Analysis

The crystallite size was calculated from the widening of the XRD reflection peak. Scherrer's formula is the simplest way of measuring the size of the crystallite, and it can only be used if the materials are not strained [53]. Thus, the X-ray line widening analysis is utilized to describe the microstructure of mechanically alloyed powders in terms of lattice strain and crystallite size. Crystal structures, crystallite sizes, and lattice strains of the as-received powders, and the obtained Al7075/4 wt.% TiC composites, were evaluated by X-ray diffraction (XRD) using a D8 ADVANCE diffractometer (Bruker AXS Inc., Fitchburg, WI, USA) with a Cu K alpha radiation source ($\lambda = 0.15406$ nm), operating at 45 kV/40 mA. The scanning range was $2\theta = 10\text{--}80^\circ$, with a step width of 0.01 and 0.02° per step as collecting time. The Bragg angles, 2θ , and the interplanar spacing (d-spacing) corresponding to the detected peaks were compared with the standard values from the International Centre for Diffraction Data's Powder Diffraction File (ICSD-53774I). The position of the peaks 2θ , its intensity hkl , and the full width at half maximum (FWHM) of the height of the peak was determined using High score Plus software. Using Scherrer's equation, the crystallite size (D) was estimated from the broadening of diffraction planes (111), (200), (220), and (311) for the Al7075 sample mentioned in Equation 1. This equation

has been utilized in previous studies [50,54]. Using the following relation, the instrumental broadening (β) corresponding to each diffraction peak was adjusted [55].

$$\beta = \sqrt{\beta_{observed}^2 - \beta_{instrumental}^2} \quad (1)$$

Peak broadening analysis utilizing the Scherrer equation was used to compute the average crystallite size.

$$D = \frac{k\lambda}{\beta \cos \theta} \quad (2)$$

where D = Crystallite size in nm, β = FWHM, $k = 0.9$, X-ray wavelength (λ) = 0.15406 nm, and θ is the peak position in radians.

Additionally, the lattice strain (ϵ) induced in powders due to imperfections in crystal and distortion was evaluated using the formula as represented in Equation (2) [50,56] as follows:

$$\epsilon = \frac{\beta}{4 \tan \theta} \quad (3)$$

2.5. Architecture of the Neural Network

For the development of the ANN model, the following steps were performed in sequence: (1) experimental data collection, (2) division of the data obtained from training, testing, and validation datasets, (3) creation of the network for the chosen parameters, (4) configuration of the network by selecting the number of hidden layers and the desired training, transfer, and necessary learning functions, and (5) training of the ANN model to acquire the MSE target by providing the required parameters. If the trials led to failure, the number of neurons of the hidden layers or weights was modified, and the network was regenerated to continue the cycle until the desired objective was achieved. Figure 2 depicts the flow chart of the ANN model framework developed to predict the crystallite size and lattice strain of the composites. The parameters for artificial neural network activity used in this study are provided in Table 3. To date, the most widely implemented neural network proposed in various studies is the multilayered neural network (MLP) [57,58]. To train a multilayered feed-forward network with multiple transfer functions for approximation, pattern identification, and pattern recognition, backpropagation learning algorithms are employed. The term backpropagation refers to the mechanism by which network error derivatives can be computed for network weights and biases. The ANN backpropagation consists of three stages: (a) feed forwarding of input data training patterns, (b) estimation and backpropagation of corresponding error, and (c) modification of weights.

Figure 3 depicts the architecture of the multi-layer perceptron (MLP) neural network utilized for the training and modeling of mechanical alloying process parameters for the fabrication of Al7075/TiC composites.

Table 3. Multilayer perceptron training and architecture parameters for this study.

Network Parameters	Values/Types
Configuration of networks	2-10-2
Neurons number in the layers	Input: 2, hidden: 10, output: 2
Hidden and output layer activation functions	Logsig (sigmoid)
Learning rules for training parameters	Backpropagation
Number of Epochs	1000

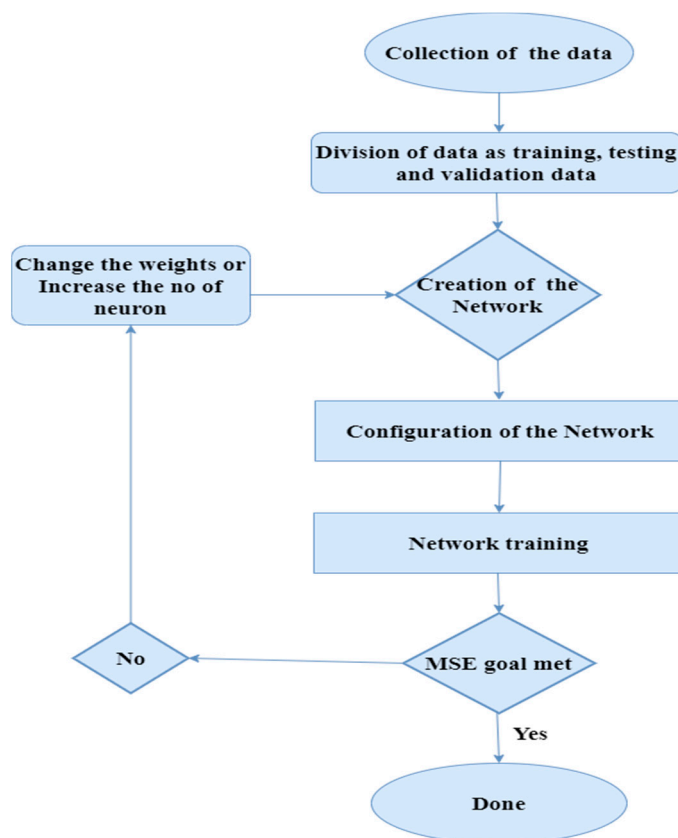


Figure 2. Proposed ANN model framework.

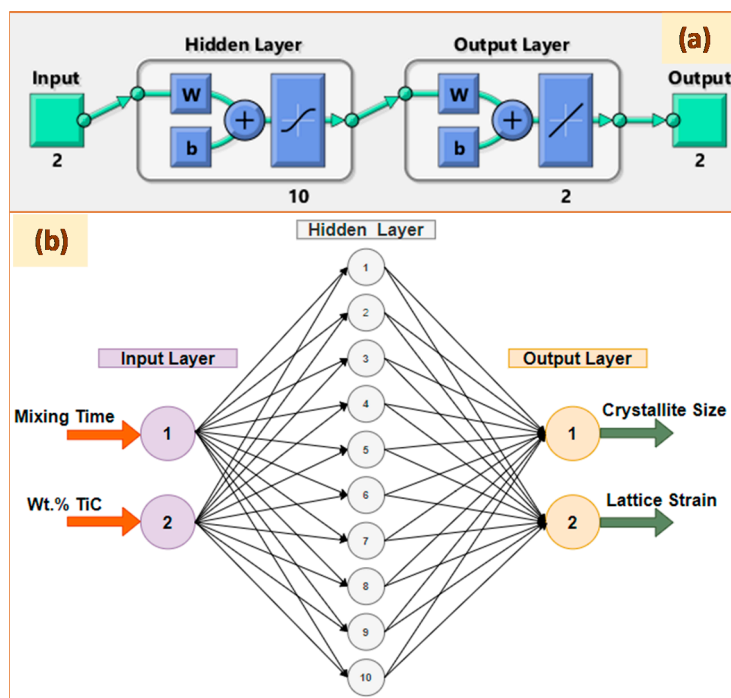


Figure 3. The ANN architecture of the three-layered neural network proposed in this study: (a) flow diagram obtained from MATLAB and (b) schematic details of the layers.

Figure 3a was derived from the MATLAB 2020b software (Mathworks®, New York, NY, USA), while Figure 3b represents the schematic details of the 2-10-2 MLP. The ANN ar-

chitecture 2-10-2 MLP is a three-layer network; the input and output layers have two nodes, while the hidden layer consists of 10 nodes. The outcomes of the neural network represent the features of the Al7075-TiC composites, namely the crystallite size and lattice strain.

3. Results and Discussion

3.1. Morphology of Received Powders

The morphological evaluation provides information on the size of the particles and the distribution of the reinforcement particles. Figure 4a,b depicts the SEM micrographs of the Al7075 and TiC powder, respectively. As observed from Figure 4a, the matrix aluminum alloy particles were spherical with varying particles sizes. The SEM morphology of the TiC particles revealed to be irregular and sharp-edged (Figure 4b). Figure 4c depicts the TEM morphology of the TiC particles. The particle size of the matrix and reinforcements was analyzed by particle size analysis, and the mean size obtained for matrix Al alloy was 15 μm with a standard deviation of 3.2 μm , whereas the TiC particles were approximately 800 nm with a standard deviation of 15.4 nm.

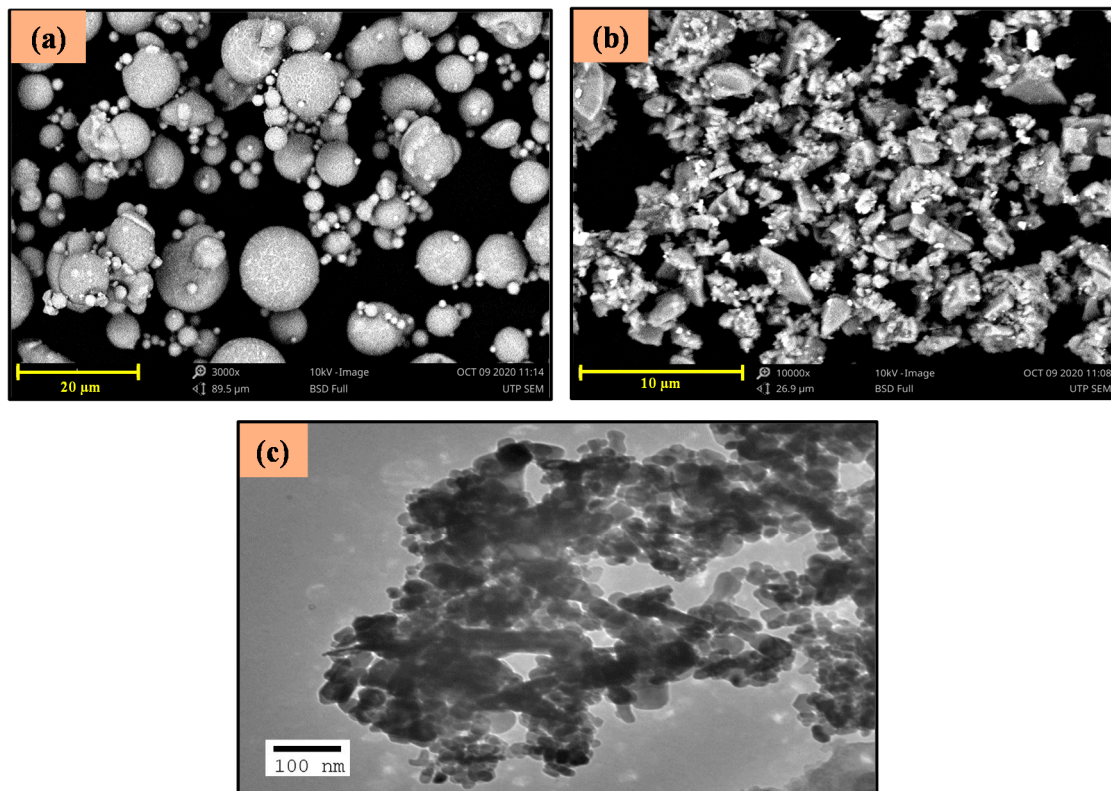


Figure 4. SEM micrographs of the received powder particles depicting (a) matrix AL7075, (b) reinforcement TiC, and (c) TEM image of TiC particles.

3.2. SEM Characterization of Composites

The Al7075 and TiC powders were mixed at various predefined milling times to obtain a uniform distribution of filler particles within the matrix. The SEM micrographs reflect the improvements in the morphology of the powders with milling time (Figures 5 and 6). It was observed that the powder size decreased with the increase in milling time. The morphologies of 3, 5, and 7 h-mixed Al7075-TiC nanocomposite powders are represented in Figures 5 and 6, in which the structure and size of Al7075 particles were shown to improve with milling time. As observed from Figure 5a,b, the Al matrix for 3-h ball milling was deformed during the early milling phase (3 h), and hard reinforcement particles were fractured due to extreme plastic deformation. Additionally, the TiC particles were agglomerated around the particles of Al7075 and distributed randomly.

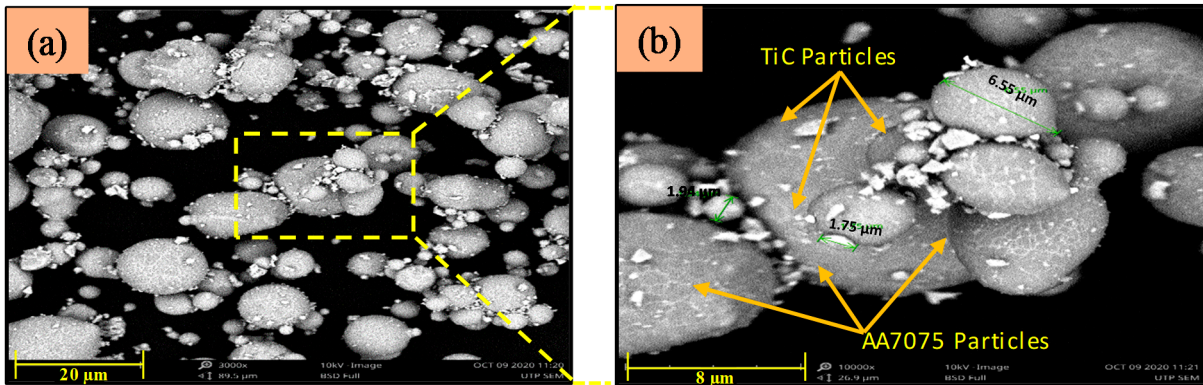


Figure 5. SEM images of the (a) 3 h-milled AL7075/4 wt.% TiC composite powder, and (b) magnified view of particle distribution for a selected region of (a).

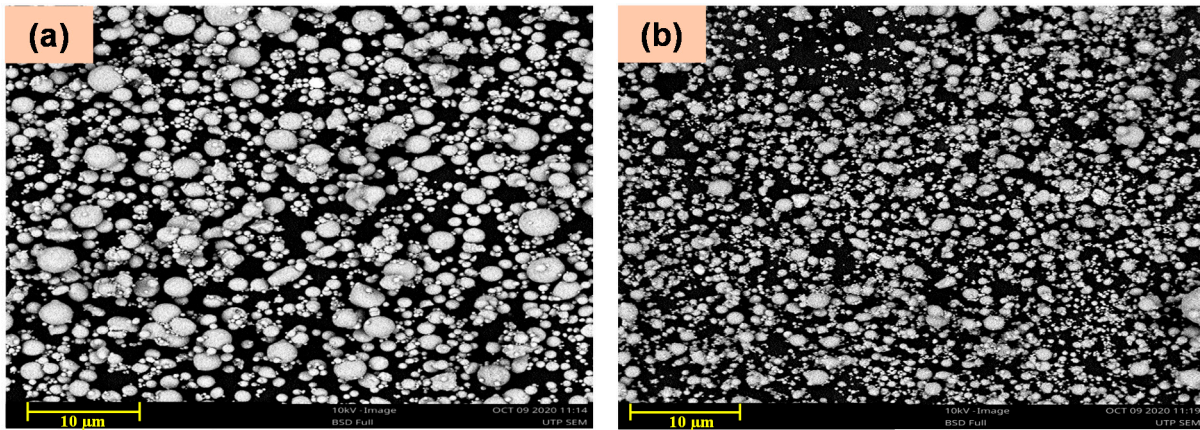


Figure 6. SEM images of the synthesized composite samples at 4 wt.% TiC compositions depicting the modifications in the morphology of the mixed powders for (a) 5 h-mixed composite powder and (b) 7 h-mixed composite powder.

However, when the milling time increased to 5 h, the composite particle size reduced, as observed in Figure 6a, and is due to friction-erosion of the AL7075 particles against the hard TiC particles. The few welded particles became fractured with a further rise in the milling period to 7 h, with both cold welding and fracturing occurring concurrently at this milling time. Hence, a mixed form of morphology with improved composite particle size was obtained as shown in Figure 6b. The particles appeared in a more equiaxed fashion, as previously observed in higher magnification images of another study [58]. As the brittle particles become distributed in a ductile matrix, the presence of hard reinforcement ceramic particles in the Al matrix composites falls into the category of a ductile-brittle component system. Thus, the ductile particles undergo deformation in the first stage of MM, while brittle particles may undergo fragmentation [22]. During the ball collision, the brittle particles among two or more ductile particles appeared as ductile particles begin to weld. Consequently, reinforcement particles would be positioned inside the welded metal particles (interfacial boundaries), resulting in the creation of an actual composite particle.

The EDS evaluation analysis of 5-h milled AL7075 + 4 wt.% TiC (Figure 7) confirmed that no contamination was induced into the composite powders throughout the milling process. Figure 8 revealed that the Al, Ti, C, Cu, Zn, and Mg peaks were the clear peaks in the selected spectrum 1. No additional peaks (Fe, Cr, Mn, or Ai) associated with AL7075 were detected due to their lower contents (below 0.2 wt.%). The EDS analysis demonstrated that, during the milling process, the powders were not contaminated. The inset image shows the deformed structure of the composite powders.

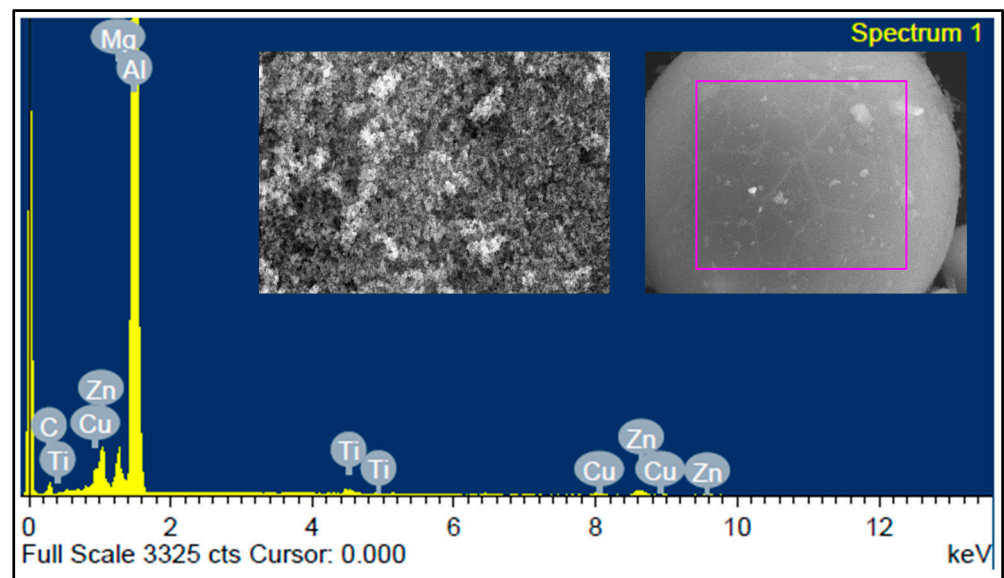


Figure 7. Analysis of Al 7075-4 wt.% TiC composite powder.

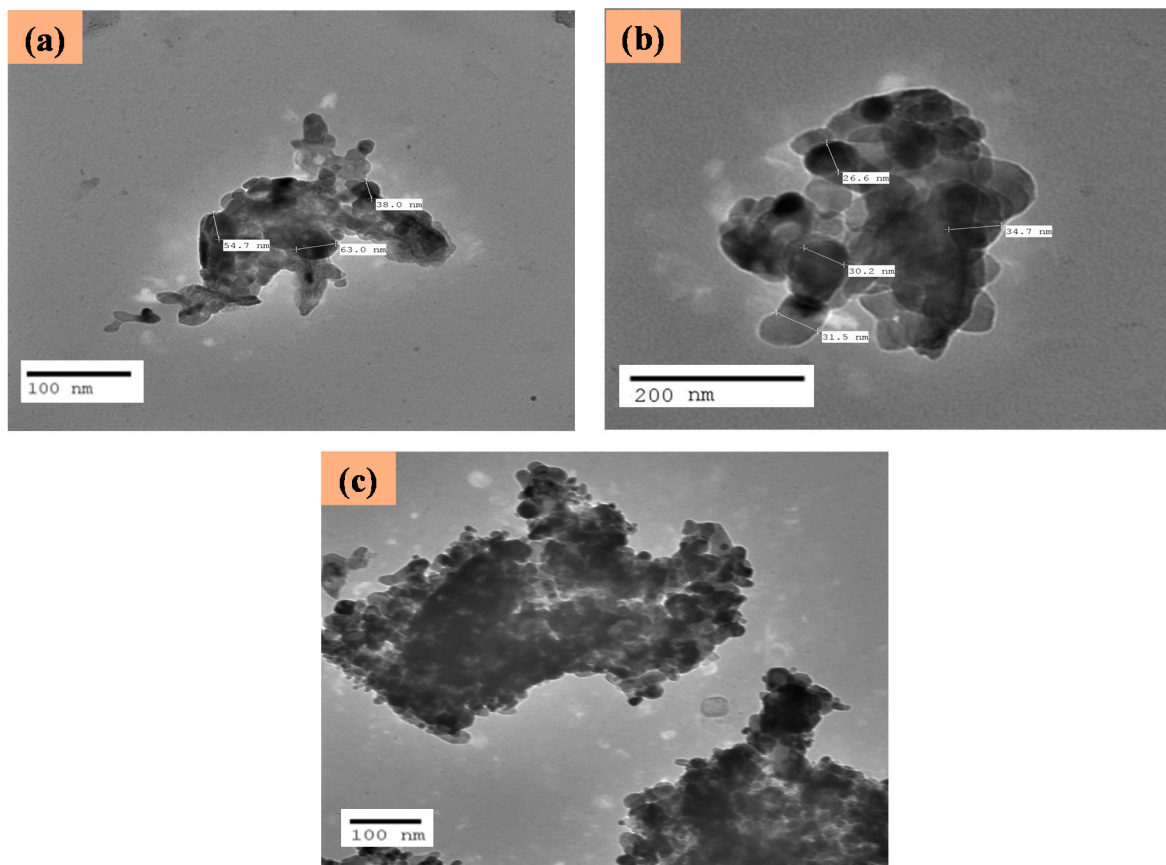


Figure 8. TEM micrographs of AL7075/4 wt.% TiC composite powder milled for: (a) 3 h, (b) 5 h, and (c) 7 h.

3.3. TEM Morphology of Composite Powder

The TEM morphology of TiC particles is depicted in Figure 4c, and the obtained morphology is in line with the existing literature of the received TiC particles TEM morphology [6,22]. The TEM micrographs of ball-milled Al7075/4 wt.% TiC powder for chosen milling time is illustrated in Figure 8. By increasing the milling time, TiC particle disper-

sion inside the Al7075 matrix is improved. As depicted in Figure 8a, TiC particles are nonuniformly distributed on the surface of the matrix Al7075 after 3 h milling. However, there was a slight improvement in the distribution for 5-h ball-milled composite powder (Figure 8b). It was observed that the TiC particles were consistently reinforced with milling time in the Al7075 matrix. The TEM morphology is in line with existing literature on the TiC-reinforced Al alloy composites [16]. Figure 8c illustrates the uniform distribution of the TiC particles, as achieved after 7 h of milling. This attributes to the good bonding between the Al7075 and TiC particles and a good cohesiveness of the Al-TiC interface. It is also reported in the literature that the distance between the particles declines with an increasing milling time [59,60]. The crystallite size of composite powder was determined using the Image J software and found to be in the range of 20–50 nm, consistent with the results obtained by the Scherrer equation. Similar TEM morphology was attained by Supriya B et al. for Al7075-TiO₂ 20-h milled composites [31].

3.4. Particle Size of Composites as a Function of Milling Time

The mean particle size of composite powder for various milling times was calculated using particle size analysis and is depicted in Figure 9.

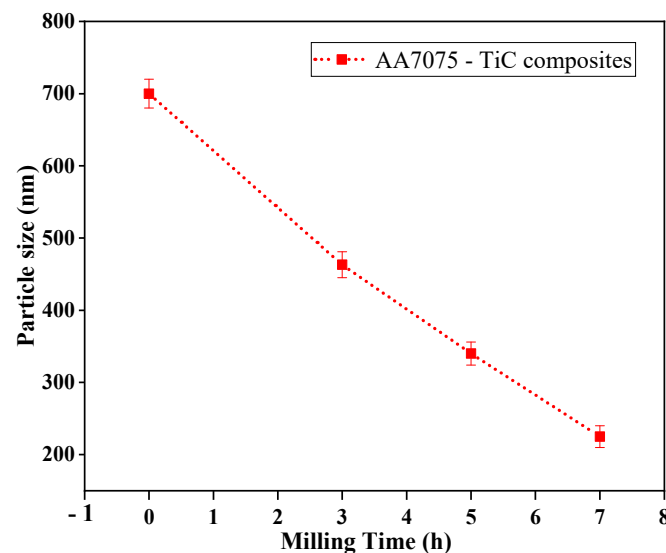


Figure 9. Effect of milling time on the size of particles determined by particle size analysis.

It was observed that, during the milling process, a decrease in particle size was observed with an increment in milling time from 3 h to 7 h. This observation is consistent with a previous study [58]. Although the milling time was limited to 7 h in this study, a critical stage may be reached using a prolonged milling time, as particles start to form a bigger cluster due to coalescence [61].

3.5. X-ray Diffraction (XRD) of the Received Powders

The XRD peak patterns of received pure aluminum alloy Al7075 and particles of TiC powders are depicted in Figures 10 and 11, respectively. As shown in Figure 10, the four major peaks of the Al matrix, (111), (200), (220), and (311), were recognized as Al with crystalline structure FCC and lattice parameters of $a = b = c = 0.4050$ nm, $\alpha = \beta = \gamma = 90^\circ$. The diffraction angles of the major peaks of Al7075 were 38.46° , 44.70° , 65.05° , and 78.14° , respectively. The XRD results for Al are consistent with the findings from other studies [46,62–64].

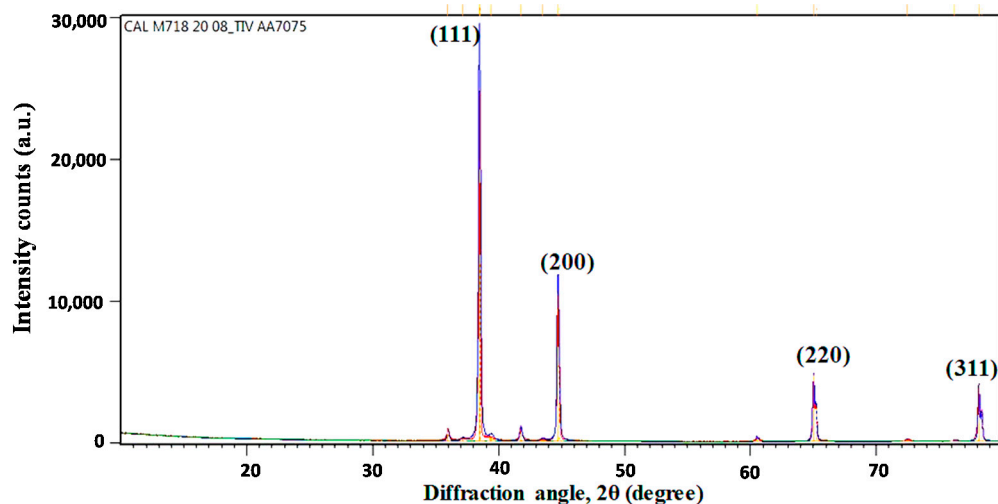


Figure 10. XRD pattern of the received matrix Al7075 powder.

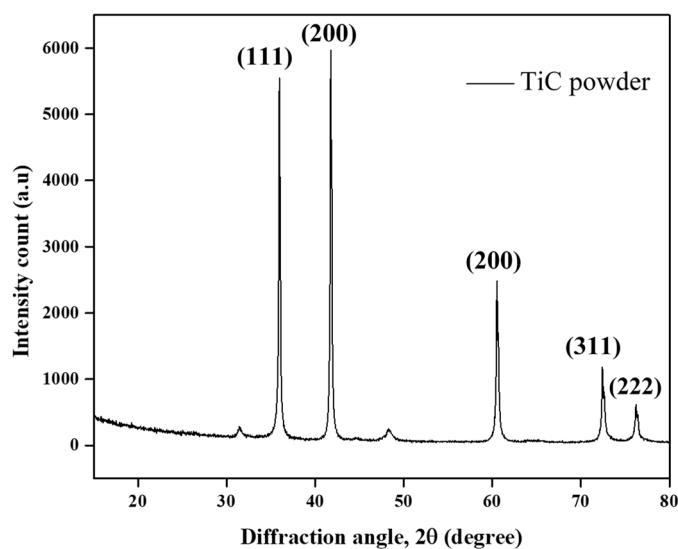


Figure 11. XRD pattern of the TiC powder.

The major peaks of TiC were identified as (111), (200), (220), (311), and (222) at diffraction angles of 35.96° , 41.76° , 60.51° , 72.49° , and 76.20° , respectively, for different TiC phases in the TiC powder (Figure 12). These results are in agreement with previous studies [16,22].

3.6. X-ray Diffraction (XRD) of the Composite Powders

Figure 12 demonstrates the XRD patterns of synthesized Al7075/4 wt.% TiC composite powders at different milling times. The planes (111), (200), (220), and (311) were identified as the peaks of Al particles. Peaks for constituent elements (Mg, Cu, Fe, Cr, and Mn) of the Al7075 alloy were not detectable in the XRD pattern due to their low volume concentration [16]. It was expected that these elements would have dispersed in the Al lattice. It was also observed that only Al and TiC phases were present, thus indicating that the synthesized powder was free from contamination.

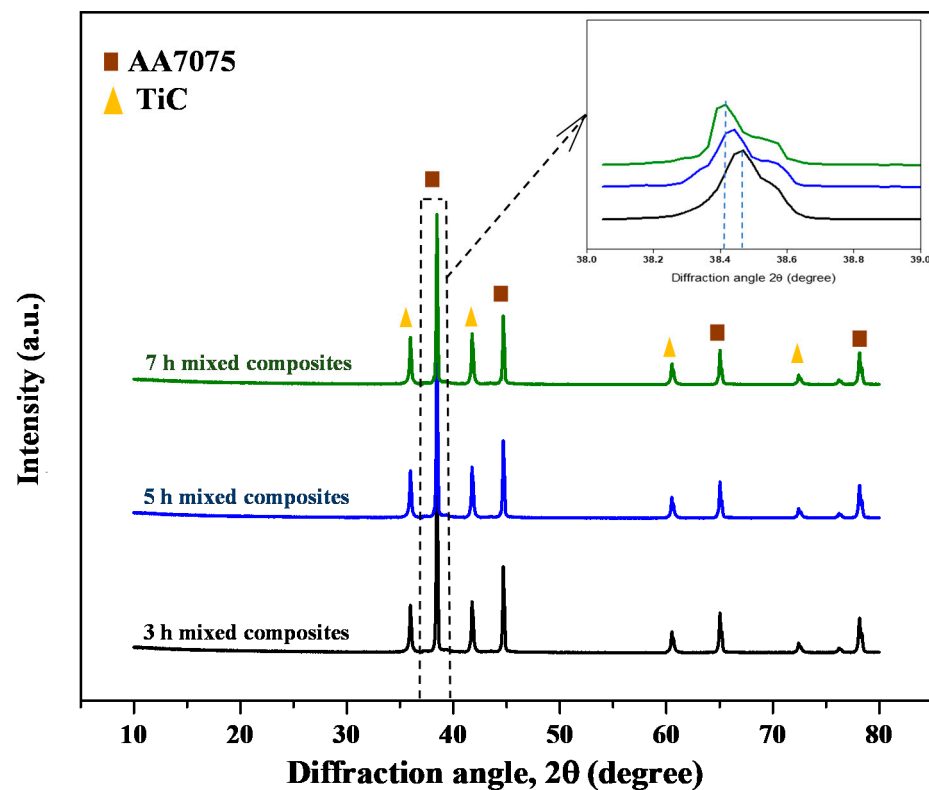


Figure 12. XRD spectrum of Al7075/4 wt.% TiC composite powders at different milling times. Insert reveals the shifts in Bragg's angle.

It was also observed from Figure 12 that the peak intensities were reduced due to the structural improvement resulting from the increment in milling time. A similar XRD pattern for Al-TiC composites was obtained by Azimi A et al. [6], for varying milling times. Additionally, the peak width of Al increased, as depicted in the inset figure. An inset of Figure 12 shows the main peak of the Al7075 matrix. The intensity reduction and peak broadening in the X-ray diffractograms reflect a decrease in crystallite size and accumulation of lattice strain, as can be observed from the inset of Figure 12, which is in good accord with the crystallite size data provided before [20]. It is also worth mentioning that the collision among composite particles on the walls of the ball mill impacts the crystallite structure of the particles.

3.7. Effect of Milling Time on the Microhardness Behavior

The combined effect of dual nature mixing time (Turbula mixing + ball milling) on the microhardness behavior was investigated for all produced composites. It was observed that the microhardness values of all synthesized composites were higher than the Al7075 matrix (Figure 13). The microhardness value for sintered Al7075 sample (C0) was observed as 62.8 HV0.5. The microhardness obtained for 1 h of the Turbula mixed sintered Al7075 + 4 wt.% TiC composite sample (C1) was observed as 67.4 HV0.5, which further improved to 76.0 HV0.5 after 3 h of ball milling of composite powder sample (sample C2). The 28.18% increment in microhardness value was observed for sample C3 (after 5 h of milling). The highest increment in the microhardness was observed as 38.4 % at 7 h of milling for sample C4. The results are in resemblance with previous studies [1,47]. It is observed from the above results that a reduction in crystallite size of the composites can be considered as one of the governing factors in the improvement of the microhardness of the Al7075/4 wt.% TiC composites. The reduction in composite crystallite sizes is achieved due to the increasing mixing time. Thus, the microhardness improvement of composite samples can also be attributed to multiple phenomena such as (i) grain refinement of the matrix Al7075

(Hall–Petch strengthening), (ii) obstacles by TiC particles during dislocations movement, and (iii) uniform distribution of TiC particles in the Al7075 matrix.

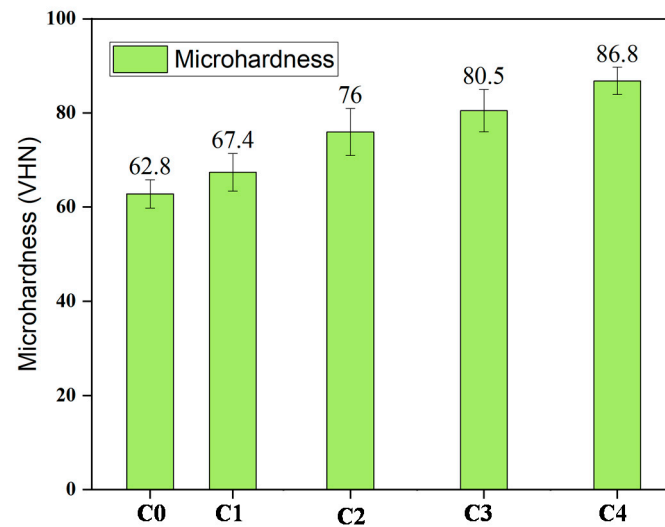


Figure 13. Effect of combined mixing time on the Vickers microhardness of synthesized composite samples.

3.8. ANN Modeling Results

The outcome predictability of the ANN simulation was calculated using mean square error (MSE). Figure 14 demonstrates the comparison between the training, validation, test, and combined datasets of real and predicted values. The precision of the model is indicated by the overall curve of performance, which is based on the correlation between the experimental and predicted results.

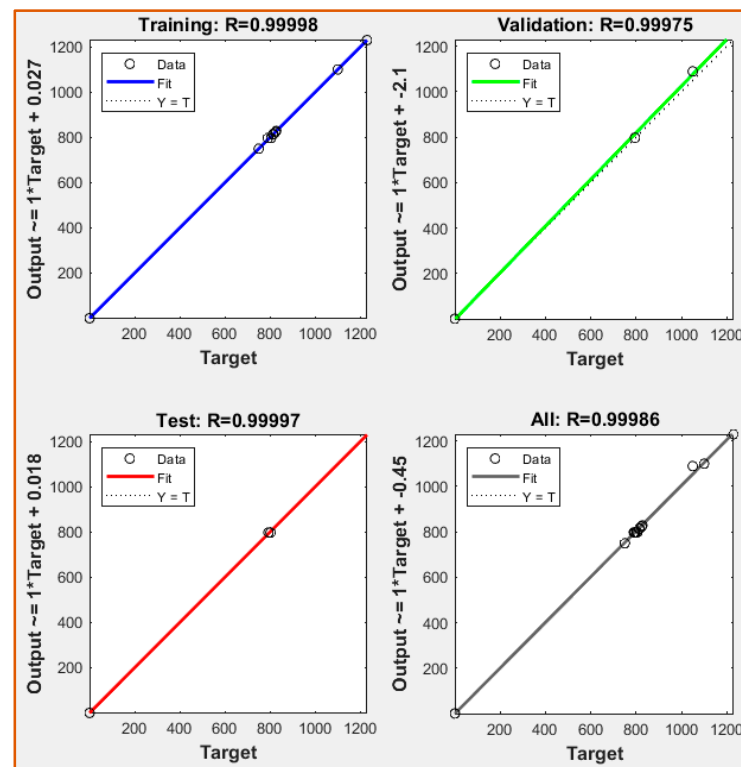


Figure 14. Regression graphs for the developed ANN network depicting training, validation, and testing.

The determination of coefficient (R) for the trained model was close to 1 ($R = 0.99998$), as depicted in Figure 14, thus indicating the successful training of the model. The regression coefficient (R), which reflects the output-target relationship, displayed an overall value of 0.99986, which was closer to 1 and signified better results. The estimated ANN values were similar to the experimental results, thus indicating a slight difference in error. Therefore, the established model can be used reliably to predict the crystallite size and lattice strain of the Al/TiC composites. Similar studies also support the effectiveness of developed ANN models for optimization of the mechanical alloying process for producing composite powder and for prediction of mechanical properties [57,65].

The mean square error (MSE) convergence during the ANN model training is depicted in Figure 15. The best validation performance was determined based on MSE during the training, where MSE convergence with a saturation value of 1.2667×10^{-3} at the 100th epoch was obtained. The best network displayed a minimum mean square error as well as a greater correlation with the experimental outcome.

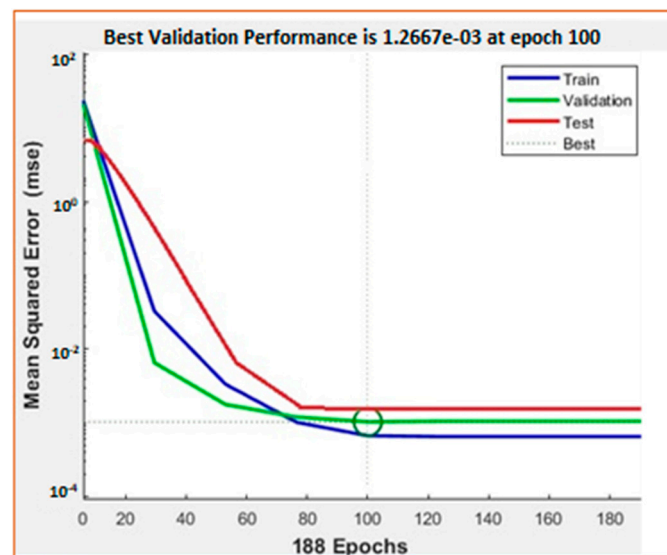


Figure 15. The curve of performance of the developed model is indicated by the mean squared error (MSE) vs. the number of epochs.

The comparison of the ANN-predicted crystallite size and experimental values are demonstrated in Figure 16. It was observed that the crystallite size predicted by the ANN model was better than experimental values. Hence, the ANN model is more appropriate for the study of the interacting variables and predictions over experimental measurements. It was found that the crystallite size of the combined blended sample (C4) with a milling time of 7 h had the least crystallite size.

Figure 17 illustrates the comparison of the response lattice strain for experimental and ANN-predicted values. The ANN-predicted lattice strain showed significantly higher values as compared to the experimental values, as observed from Figure 17. Thus, the ANN model was consistent with the experimental results.

A comparison of the experimental and ANN-predicted data for the three best prediction models has been analyzed by comparing the statistical errors (mean absolute percentage error “MAPE” and root mean square error “RMSE”), as illustrated in Table 4.

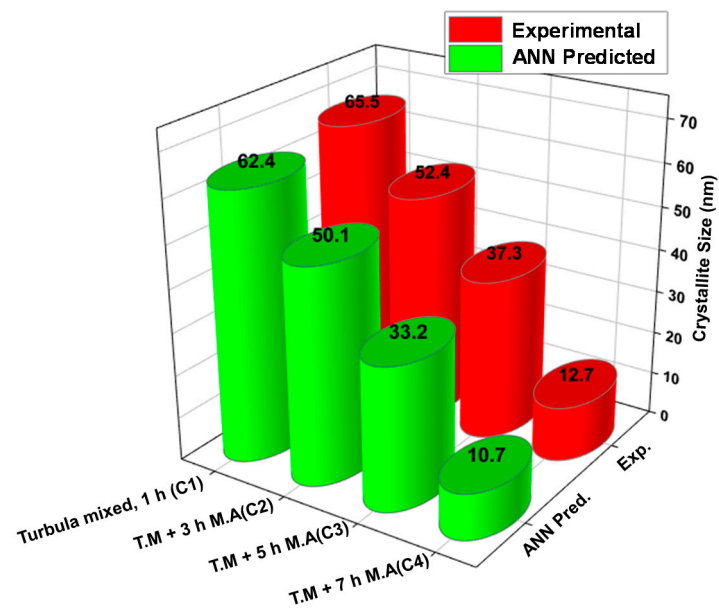


Figure 16. Variation in crystallite size for the experimental and ANN-predicted values as a function of milling time.

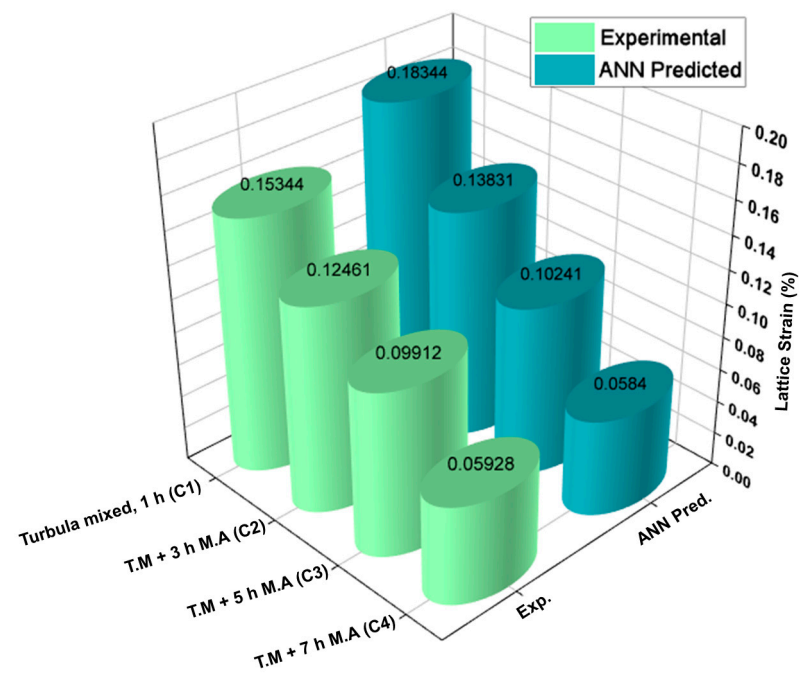


Figure 17. Comparison of the lattice strain (%) with experimental and ANN-predicted values as a function of milling time.

Table 4. MAPE and RMSE values for the three best prediction models.

Error Prediction	Crystallite Size	Lattice Strain
RMSE	3.34	3.45
MAPE	2.84	1.45

4. Conclusions and Future Scope

In this study, aluminum-based composites Al7075/4 wt.% TiC were synthesized using a two-stage blending process (Turbula mixing and ball milling). The synthesized composite

powders were characterized by XRD, SEM, EDS, and TEM techniques. The effect of milling time on the crystallite size and lattice strain was investigated. Additionally, an ANN-based model was developed to predict the crystallite size and lattice strain of the blended composite powders. The key conclusions of this study are as follows:

- The two-stage blending of composite powders resulted in good incorporation and uniform dispersion of TiC particle reinforcement in the Al7075 powder matrix. The SEM and TEM micrographs of the synthesized composite powders confirm the homogeneous distribution of reinforcement into the matrix.
- Al7075-TiC composite powder XRD patterns have been verified since there were no intermetallic compounds, even after 7 h of ball milling. With this milling period (i.e., 7 h), the decrement in Al7075 peaks indicates its dissolution in reinforcement TiC, thus causing lattice distortion that results in peaks expanding and shifting.
- With an increase in milling time, a decrease in average crystallite size is achieved, and the minimum crystallite size of 12.7 nm is attained for all composites at 7 h of milling time. Lattice strain increased significantly with milling time; the maximum value achieved at 7 h was 0.1534 %.
- Rising milling time gradually (from 3 h to 7 h) activated the deformation hardening mechanism and consequently resulted in an improvement in the microhardness values of the synthesized composites. The results of microhardness measurements revealed that the highest increment in the microhardness of synthesized composites was observed as 38.4 % at 7 h of milling for sample C4. The microhardness of the composite samples was higher as compared to the unreinforced Al7075 matrix. Thus, increasing ball milling is beneficial for the homogeneous dispersion of TiC particles within the Al7075 matrix.
- A backpropagation-based ANN model was developed to predict the crystallite size and lattice strain of the synthesized composites. The ANN model results are in good agreement with the experimental results. Moreover, the developed ANN model can be used as a tool in predicting composite lattice parameters and other related properties. Thus, the ANN is an effective method for estimating the lattice parameters of Al7075–TiC composites produced by the mechanical alloying method.
- The limitation of the present work is the small range of milling time and limited characteristics (crystallite size, lattice strain, and microhardness behavior) studies. However, the effect of different process variables viz., sintering temperature, compaction pressure, and dwell time on the physical, mechanical, and tribological characteristics of powder metallurgy processed Al7075/TiC composites can be investigated and predicted by some other machine learning techniques. It is also recommended to extend the present study by increasing the milling time with same experimental boundary conditions.

Author Contributions: Conceptualization, M.A.A.; funding acquisition, H.H.Y.; investigation, M.A.A. and I.A.S. (Imtiaz Ahmed Shozib); methodology, M.A.A., M.A. and I.A.S. (Imtiaz Ali Soomro); software, M.Y.; supervision, H.H.Y. and S.M.S.; writing—review and editing, M.A.A., H.H.Y., F.M. and J.A. All authors have read and agreed to the published version of the manuscript.

Funding: This research was funded by the Universiti Teknologi PETRONAS grant (YUTP-FRG 1/2021), grant number (015LCO-339).

Institutional Review Board Statement: Not applicable.

Informed Consent Statement: Not applicable.

Data Availability Statement: Not applicable.

Acknowledgments: The authors also acknowledge the Universiti Teknologi Petronas, Malaysia for providing all research lab facilities required for the investigations. Also, for providing financial assistantship under Graduate Research Assistantship (GRA) scheme.

Conflicts of Interest: The authors declare no conflict of interest.

References

1. Almotairy, S.M.; Alharthi, N.H.; Alharbi, H.F.; Abdo, H.S. Superior Mechanical Performance of Inductively Sintered Al/SiC Nanocomposites Processed by Novel Milling Route. *Sci. Rep.* **2020**, *10*, 10368. [[CrossRef](#)] [[PubMed](#)]
2. Alam, M.A.; Ya, H.H.; Sapuan, S.M.; Mamat, O.; Parveez, B.; Yusuf, M.; Masood, F.; Ilyas, R.A. *Recent Advancements in Advanced Composites for Aerospace Applications: A Review BT—Advanced Composites in Aerospace Engineering Applications*; Mazlan, N., Sapuan, S.M., Ilyas, R.A., Eds.; Springer International Publishing: Cham, Switzerland, 2022; pp. 319–339. ISBN 978-3-030-88192-4. [[CrossRef](#)]
3. Asyraf, M.R.M.; Ilyas, R.A.; Sapuan, S.M.; Harussani, M.M.; Hariz, H.M.; Aiman, J.M.; Baitaba, D.M.; Sanjay, M.R.; Ishak, M.R.; Norkhairunnisa, M.; et al. *Advanced Composite in Aerospace Applications: Opportunities, Challenges, and Future Perspective BT—Advanced Composites in Aerospace Engineering Applications*; Mazlan, N., Sapuan, S.M., Ilyas, R.A., Eds.; Springer International Publishing: Cham, Switzerland, 2022; pp. 471–498. ISBN 978-3-030-88192-4. [[CrossRef](#)]
4. Alam, M.A.; Asoushe, M.H.; Pourhakkak, P.; Gritsch, L.; Alipour, A.; Mohammadi, S. Preparation of bioactive polymer-based composite by different techniques and application in tissue engineering: A review. *J. Compos. Compd.* **2021**, *3*, 194–205. [[CrossRef](#)]
5. Alam, M.A.; Ya, H.H.; Ahmad, A.; Yusuf, M.; Azeem, M.; Masood, F. Influence of aluminum addition on the mechanical properties of brass/Al composites fabricated by stir casting. *Mater. Today Proc.* **2022**, *48*, 811–814. [[CrossRef](#)]
6. Azimi, A.; Shokuhfar, A.; Nejadseyfi, O. Mechanically alloyed Al7075—TiC nanocomposite: Powder processing, consolidation and mechanical strength. *Mater. Des.* **2015**, *66*, 137–141. [[CrossRef](#)]
7. Arsun, O.; Akgul, Y.; Simsir, H. Investigation of the properties of Al7075-HTC composites produced by powder metallurgy. *J. Compos. Mater.* **2021**, *55*, 2339–2348. [[CrossRef](#)]
8. Ezatpour, H.R.; Torabi Parizi, M.; Sajjadi, S.A.; Ebrahimi, G.R.; Chaichi, A. Microstructure, mechanical analysis and optimal selection of 7075 aluminum alloy based composite reinforced with alumina nanoparticles. *Mater. Chem. Phys.* **2016**, *178*, 119–127. [[CrossRef](#)]
9. Al-Salihi, H.A.; Mahmood, A.A.; Alalkawi, H.J. Mechanical and wear behavior of AA7075 aluminum matrix composites reinforced by Al₂O₃ nanoparticles. *Nanocomposites* **2019**, *5*, 67–73. [[CrossRef](#)]
10. Alam, M.A.; Sapuan, S.M.; Ya, H.H.; Hussain, P.B.; Azeem, M.; Ilyas, R.A. Application of biocomposites in automotive components: A review. In *Biocomposite and Synthetic Composites for Automotive Applications*; Elsevier: Amsterdam, The Netherlands, 2021; pp. 1–17. [[CrossRef](#)]
11. Feijoo, I.; Cabeza, M.; Merino, P.; Pena, G.; Pérez, M.C.; Cruz, S.; Rey, P. Estimation of crystallite size and lattice strain in nano-sized TiC particle-reinforced 6005A aluminium alloy from X-ray diffraction line broadening. *Powder Technol.* **2019**, *343*, 19–28. [[CrossRef](#)]
12. Hadian, M.; Shahrajabian, H.; Ra, M. Mechanical properties and microstructure of Al/(TiC + TiB₂) composite fabricated by spark plasma sintering. *Ceram. Int.* **2019**, *45*, 12088–12092. [[CrossRef](#)]
13. Ramkumar, K.R.; Sivasankaran, S.; Al-mufadi, F.A.; If, T.D.; Siddharth, S. ScienceDirect Investigations on microstructure, mechanical, and tribological behaviour of AA 7075—x wt. % TiC composites for aerospace applications. *Arch. Civ. Mech. Eng.* **2019**, *19*, 428–438. [[CrossRef](#)]
14. Baek, M.S.; Euh, K.; Lee, K.A. Microstructure, tensile and fatigue properties of high strength Al 7075 alloy manufactured via twin-roll strip casting. *J. Mater. Res. Technol.* **2020**, *9*, 9941–9950. [[CrossRef](#)]
15. Azeem, M.; Ya, H.H.; Alam, M.A.; Kumar, M.; Stabla, P.; Smolnicki, M.; Gemi, L.; Khan, R.; Ahmed, T.; Ma, Q.; et al. Application of Filament Winding Technology in Composite Pressure Vessels and Challenges: A Review. *J. Energy Storage* **2022**, *49*, 103468. [[CrossRef](#)]
16. Jeyasimman, D.; Sivasankaran, S.; Sivaprasad, K.; Narayanasamy, R.; Kambali, R.S. An investigation of the synthesis, consolidation and mechanical behaviour of Al 6061 nanocomposites reinforced by TiC via mechanical alloying. *Mater. Des.* **2014**, *57*, 394–404. [[CrossRef](#)]
17. Moorthy, C.V.K.N.S.N.; Kumar, G.N.; Srinivas, V.; Kumar, M.A.; Reddy, K.R.R.M.; Vasundhara, D.N.; Sabri, M.F.M.; Said, S.M. Metallography, Microstructure, and Wear Analysis of AA 6063/TiC Composites for Augmented Dry Sliding Property at Room Temperature. *Metallogr. Microstruct. Anal.* **2020**, *9*, 140–151. [[CrossRef](#)]
18. Mohapatra, S.; Chaubey, A.K.; Mishra, D.K.; Singh, S.K. Fabrication of Al—TiC composites by hot consolidation technique: Its microstructure and mechanical properties. *Integr. Med. Res.* **2015**, *5*, 117–122. [[CrossRef](#)]
19. Popov, V.A.; Burghammer, M.; Rosenthal, M.; Kotov, A. In situ synthesis of TiC nano-reinforcements in aluminum matrix composites during mechanical alloying. *Compos. Part B Eng.* **2018**, *145*, 57–61. [[CrossRef](#)]
20. Hernández-Martínez, S.E.; Cruz-Rivera, J.J.; Garay-Reyes, C.G.; Martínez-Sánchez, R.; Estrada-Guel, I.; Hernández-Rivera, J.L. Comparative study of synthesis of AA 7075-ZrO₂ metal matrix composite by different mills. *J. Alloys Compd.* **2015**, *643*, S107–S113. [[CrossRef](#)]
21. Estrada-Guel, I.; Carreño-Gallardo, C.; Mendoza-Ruiz, D.C.; Miki-Yoshida, M.; Rocha-Rangel, E.; Martínez-Sánchez, R. Graphite nanoparticle dispersion in 7075 aluminum alloy by means of mechanical alloying. *J. Alloys Compd.* **2009**, *483*, 173–177. [[CrossRef](#)]
22. Cabeza, M.; Feijoo, I.; Merino, P.; Pena, G.; Pérez, M.C.; Cruz, S.; Rey, P. Effect of high energy ball milling on the morphology, microstructure and properties of nano-sized TiC particle-reinforced 6005A aluminium alloy matrix composite. *Powder Technol.* **2017**, *321*, 31–43. [[CrossRef](#)]

23. Alam, M.; Ya, H.; Azeem, M.; Yusuf, M.; Sapuan, S.; Masood, F. Investigating the effect of mixing time on the crystallite size and lattice strain of the AA7075/TiC composites. *Mater. Werkst.* **2021**, *52*, 1112–1120. [[CrossRef](#)]
24. Ghasali, E.; Fazili, A.; Alizadeh, M.; Shirvanimoghaddam, K. Evaluation of Microstructure and Mechanical Properties of Al-TiC Metal Matrix Composite Prepared by Conventional, Microwave and Spark. *Materials* **2017**, *10*, 1255. [[CrossRef](#)] [[PubMed](#)]
25. Fouly, A.; Almotairy, S.M.; Aijaz, M.O.; Alharbi, H.F.; Abdo, H.S. Balanced mechanical and tribological performance of high-frequency-sintered al-sic achieved via innovative milling route—Experimental and theoretical study. *Crystals* **2021**, *11*, 700. [[CrossRef](#)]
26. Hamed, A.T.; Mosa, E.S.; Mahdy, A.; El-Batanony, I.G.; Elkady, O.A. Preparation and evaluation of cu-zn-gnss nanocomposite manufactured by powder metallurgy. *Crystals* **2021**, *11*, 1449. [[CrossRef](#)]
27. Esmati, M.; Sharifi, H.; Raesi, M.; Atrian, A.; Rajaei, A. Investigation into thermal expansion coefficient, thermal conductivity and thermal stability of Al-graphite composite prepared by powder metallurgy. *J. Alloys Compd.* **2019**, *773*, 503–510. [[CrossRef](#)]
28. Akinwamide, S.O.; Lesufi, M.; Akinribide, O.J.; Mpolo, P.; Olubambi, P.A. Evaluation of microstructural and nanomechanical performance of spark plasma sintered TiFe-SiC reinforced aluminium matrix composites. *J. Mater. Res. Technol.* **2020**, *9*, 12137–12148. [[CrossRef](#)]
29. Singh, L.K.; Bhadauria, A.; Laha, T. Al-MWCNT nanocomposite synthesized via spark plasma sintering: Effect of powder milling and reinforcement addition on sintering kinetics and mechanical properties. *J. Mater. Res. Technol.* **2019**, *8*, 503–512. [[CrossRef](#)]
30. Kushwaha, A.K.; John, M.; Misra, M.; Menezes, P.L. Nanocrystalline Materials: Synthesis, Characterization, Properties, and Applications. *Crystals* **2021**, *11*, 1317. [[CrossRef](#)]
31. Bera, S.; Chowdhury, S.G.; Estrin, Y.; Manna, I. Mechanical properties of Al7075 alloy with nano-ceramic oxide dispersion synthesized by mechanical milling and consolidated by equal channel angular pressing. *J. Alloys Compd.* **2013**, *548*, 257–265. [[CrossRef](#)]
32. Ahamed, H.; Senthilkumar, V. Role of nano-size reinforcement and milling on the synthesis of nano-crystalline aluminium alloy composites by mechanical alloying. *J. Alloys Compd.* **2010**, *505*, 772–782. [[CrossRef](#)]
33. Obadele, B.A.; Masuku, Z.H.; Olubambi, P.A. Turbula mixing characteristics of carbide powders and its influence on laser processing of stainless steel composite coatings. *Powder Technol.* **2012**, *230*, 169–182. [[CrossRef](#)]
34. Sulima, I.; Hyjek, P.; Podsiadło, M. Fabrication of the zirconium diboride-reinforced composites by a combination of planetary ball milling, turbula mixing and spark plasma sintering. *Materials* **2021**, *14*, 4056. [[CrossRef](#)]
35. Kulecki, P.; Lichańska, E. The Effect of Powder Ball Milling on the Microstructure and Mechanical Properties of Sintered Fe-Cr-Mo-Mn-(Cu) Steel. *Powder Metall. Prog.* **2017**, *17*, 82–92. [[CrossRef](#)]
36. Abd Elhamid, M.; Emara, M.M.; Salem, H.G. Influence of mixing technique on the mechanical properties and structural evolution of Al-NiAl Composites. *J. Mater. Eng. Perform.* **2014**, *23*, 3425–3435. [[CrossRef](#)]
37. Hafeez, A.; Ammar Taqvi, S.A.; Fazal, T.; Javed, F.; Khan, Z.; Amjad, U.S.; Bokhari, A.; Shehzad, N.; Rashid, N.; Rehman, S.; et al. Optimization on cleaner intensification of ozone production using Artificial Neural Network and Response Surface Methodology: Parametric and comparative study. *J. Clean. Prod.* **2020**, *252*, 119833. [[CrossRef](#)]
38. Roohi, R.; Jafari, M.; Jahantab, E.; Aman, M.S.; Moameri, M.; Zare, S. Application of artificial neural network model for the identification of the effect of municipal waste compost and biochar on phytoremediation of contaminated soils. *J. Geochem. Explor.* **2020**, *208*, 106399. [[CrossRef](#)]
39. Varol, T.; Canakci, A.; Ozsahin, S. Artificial neural network modeling to effect of reinforcement properties on the physical and mechanical properties of Al2024-B4C composites produced by powder metallurgy. *Compos. Part B Eng.* **2013**, *54*, 224–233. [[CrossRef](#)]
40. Amirjan, M.; Khorsand, H.; Siadati, M.H.; Eslami Farsani, R. Artificial Neural Network prediction of Cu-Al2O3 composite properties prepared by powder metallurgy method. *J. Mater. Res. Technol.* **2013**, *2*, 351–355. [[CrossRef](#)]
41. Dewangan, S.K.; Samal, S.; Kumar, V. Microstructure exploration and an artificial neural network approach for hardness prediction in AlCrFeMnNiWx High-Entropy Alloys. *J. Alloys Compd.* **2020**, *823*, 153766. [[CrossRef](#)]
42. Durmuş, H.K.; Özkaya, E.; Meri, C. The use of neural networks for the prediction of wear loss and surface roughness of AA 6351 aluminium alloy. *Mater. Des.* **2006**, *27*, 156–159. [[CrossRef](#)]
43. Arif, S.; Alam, M.T.; Ansari, A.H.; Shaikh, M.B.N.; Siddiqui, M.A. Analysis of tribological behaviour of zirconia reinforced Al-SiC hybrid composites using statistical and artificial neural network technique. *Mater. Res. Express* **2018**, *5*, 056506. [[CrossRef](#)]
44. Nwobi-Okoye, C.C.; Ochieze, B.Q. Age hardening process modeling and optimization of aluminum alloy A356/Cow horn particulate composite for brake drum application using RSM, ANN and simulated annealing. *Def. Technol.* **2018**, *14*, 336–345. [[CrossRef](#)]
45. Varol, T.; Canakci, A.; Ozsahin, S. Prediction of effect of reinforcement content, flake size and flake time on the density and hardness of flake AA2024-SiC nanocomposites using neural networks. *J. Alloys Compd.* **2018**, *739*, 1005–1014. [[CrossRef](#)]
46. Alam, M.A.; Ya, H.H.; Azeem, M.; Hussain, P.B.; Sapuan, S.M.; Khan, R.; Arif, S.; Ansari, A.H. Modelling and optimisation of hardness behaviour of sintered Al/SiC composites using RSM and ANN: A comparative study. *J. Mater. Res. Technol.* **2020**, *9*, 14036–14050. [[CrossRef](#)]
47. Ahmed, I.; Ahmad, A.; Rahaman, S.A.; Abdul-rani, A.; Azad, M. Modelling and optimization of microhardness of electroless Ni-P-TiO₂ composite coating based on machine learning approaches and RSM. *J. Mater. Res. Technol.* **2021**, *12*, 1010–1025. [[CrossRef](#)]

48. Erturun, V.; Çetin, S.; Sahin, O. Investigation of Microstructure of Aluminum Based Composite Material Obtained by Mechanical Alloying. *Met. Mater. Int.* **2020**, *27*, 1662–1670. [[CrossRef](#)]
49. Jiang, J.; Shen, Y.; Feng, X. Microstructures evolution, formation mechanisms and properties of Sicp/ Al composite coatings on Ti-6Al-4v substrate via mechanical alloying method. *Surf. Interfaces* **2020**, *19*, 100487. [[CrossRef](#)]
50. Zawrah, M.F.; Abdel-Kader, H.; Elbaly, N.E. Fabrication of Al₂O₃-20 vol. % Al nanocomposite powders using high energy milling and their sinterability. *Mater. Res. Bull.* **2012**, *47*, 655–661. [[CrossRef](#)]
51. Surya, M.S.; Prasanthi, G.; Kumar, A.K.; Sridhar, V.K.; Gugulothu, S.K. Optimization of Tribological Properties of Powder Metallurgy-Processed Aluminum7075/SiC Composites Using ANOVA and Artificial Neural Networks. *J. Bio- Tribo-Corros.* **2021**, *7*, 161. [[CrossRef](#)]
52. Zhang, Y.F.; Lu, L.; Yap, S.M. Prediction of the amount of PCA for mechanical milling. *J. Mater. Process. Technol.* **1999**, 89–90, 260–265. [[CrossRef](#)]
53. Cullity, B.D. *Answers to Problems: Elements of X-ray Diffraction*; Addison-Wesley Publishing Company: Boston, MA, USA, 1978; ISBN 0201089173.
54. Sivasankaran, S.; Sivaprasad, K.; Narayanasamy, R.; Satyanarayana, P.V. X-ray peak broadening analysis of AA 6061100-x-x wt.% Al₂O₃ nanocomposite prepared by mechanical alloying. *Mater. Charact.* **2011**, *62*, 661–672. [[CrossRef](#)]
55. Rajesh Kumar, B.; Hymavathi, B. X-ray peak profile analysis of solid-state sintered alumina doped zinc oxide ceramics by Williamson–Hall and size-strain plot methods. *J. Asian Ceram. Soc.* **2017**, *5*, 94–103. [[CrossRef](#)]
56. Zawrah, M.F.; Zayed, H.A.; Essawy, R.A.; Nassar, A.H.; Taha, M.A. Preparation by mechanical alloying, characterization and sintering of Cu-20wt.% Al₂O₃ nanocomposites. *Mater. Des.* **2013**, *46*, 485–490. [[CrossRef](#)]
57. Dashtbayazi, M.R.; Shokuhfar, A.; Simchi, A. Artificial neural network modeling of mechanical alloying process for synthesizing of metal matrix nanocomposite powders. *Mater. Sci. Eng. A* **2007**, *466*, 274–283. [[CrossRef](#)]
58. Sethi, J.; Das, S.; Das, K. Evaluating the influence of milling time, and sintering temperature and time on the microstructural changes and mechanical properties of Al-Y2W3O12-AlN hybrid composites. *Powder Technol.* **2021**, *377*, 244–256. [[CrossRef](#)]
59. Sohi, M.H.; Hojjatzadeh, S.M.H.; Moosavifar, S.S.; Heshmati-Manesh, S. Liquid phase surface melting of AA8011 aluminum alloy by addition of Al/Al₂O₃ nano-composite powders synthesized by high-energy milling. *Appl. Surf. Sci.* **2014**, *313*, 76–84. [[CrossRef](#)]
60. Jeyasimman, D.; Sivaprasad, K.; Sivasankaran, S.; Ponalagusamy, R.; Narayanasamy, R.; Iyer, V. Microstructural observation, consolidation and mechanical behaviour of AA 6061 nanocomposites reinforced by γ -Al₂O₃ nanoparticles. *Adv. Powder Technol.* **2015**, *26*, 139–148. [[CrossRef](#)]
61. Nath, A.K.; Jiten, C.; Singh, K.C. Influence of ball milling parameters on the particle size of barium titanate nanocrystalline powders. *Phys. B Condens. Matter* **2010**, *405*, 430–434. [[CrossRef](#)]
62. Michael Rajan, H.B.; Ramabalan, S.; Dinaharan, I.; Vijay, S.J. Synthesis and characterization of in situ formed titanium diboride particulate reinforced AA7075 aluminum alloy cast composites. *Mater. Des.* **2013**, *44*, 438–445. [[CrossRef](#)]
63. Arif, S.; Alam, T.; Ansari, A.H.; Bilal, M.; Shaikh, N. Morphological characterization, statistical modelling and tribological behaviour of aluminum hybrid nanocomposites reinforced with micro-nano-silicon carbide. *J. Asian Ceram. Soc.* **2019**, *7*, 434–448. [[CrossRef](#)]
64. Yusuf, M.; Farooqi, A.S.; Keong, L.K.; Hellgardt, K.; Abdullah, B. Contemporary trends in composite Ni-based catalysts for CO₂ reforming of methane. *Chem. Eng. Sci.* **2021**, *229*, 116072. [[CrossRef](#)]
65. Jain, R.; Dewangan, S.K.; Kumar, V.; Samal, S. Artificial neural network approach for microhardness prediction of eight component FeCoNiCrMnVAlNb eutectic high entropy alloys. *Mater. Sci. Eng. A* **2020**, *797*, 140059. [[CrossRef](#)]